Available online at https://link.springer.com/journal/42241
http://www.jhydrodynamics.com
Journal of Hydrodynamics, 2023, 35(4): 724-735
https://doi.org/10.1007/s42241-023-0057-4

Numerical investigations of focused wave interact with a moving cylinder

Yuan Zhuang[1], Fu-chang Zhou[2], Wen-jun Zhou[3], De-cheng Wan[1*]
1. *Computational Marine Hydrodynamics Lab (CMHL), School of Naval Architecture, Ocean and Civil Engineering, Shanghai Jiao Tong University, Shanghai 200240, China*
2. *Wuhan Second Ship Design and Research Institute, Wuhan 430205, China*
3. *Marine Design and Research Institute of China, Shanghai 200011, China*

(Received September 10, 2023, Revised September 17, 2023, Accepted September 18, 2023, Published online October 20, 2023)

Abstract: This paper presents a numerical study on focused wave and current interactions with a cylinder. The cylinder is moving in the opposite direction to the wave propagation. An effective computational decomposition method is adopted to reduce the calculation resources. A potential solver high-order spectral (HOS) method is applied to generate focused wave field, while our in-house computational fluid dynamics (CFD) solver naoe-FOAM-SJTU with overset grid takes the charge of achieving the viscous effect around the moving cylinder. The viscous domain moving with the cylinder thus the size and mesh grids in computational domain is greatly reduced. The pressure on cylinder surface and wave fields around cylinder are compared with experimental data, shows a well agreement. Meanwhile, the scattering wave field and vortex shedding are discussed. With the existence of moving cylinder, the classical scattering wave types are still observed.

Key words: Focused wave, moving cylinder, naoe-FOAM-SJTU solver, computational decomposition method

0. Introduction

The monopile is a common structure in costal or wind turbine construction. As the bottom fixed, the monopile would be exposed to severe sea states such as rouge waves or rough wave interacts with current. This may bring huge damage on structures and complicated hydrodynamic characteristics. When the monopile encountered with rouge wave with current, the wave-wave and wave-current-structure interaction need to be considered.

In past decades, large amount studies on interaction between waves and cylinder have been carried out. Most of the studies were based on Morison equation which predicted inertia and drag forces well but cannot include radiated or scattering waves[1]. This might lead to wrong results when steep waves interacted with cylinders. Meanwhile, breaking phenomenon might happen when steep waves interacted with the cylinder, which brought impact pressure on cylinders.

Project supported by the National Natural Science Foundation of China (Grant Nos. 52201372, 52131102).
Biography: Yuan Zhuang (1993-), Female, Ph. D.,
E-mail: nana2_0@sjtu.edu.cn
Corresponding author: De-cheng Wan,
E-mail: dcwan@sjtu.edu.cn

The researches of steep wave-structure interaction turned from high-order regular waves[2] to focused waves. The focused waves are the idealized concept to mimic the sudden and huge wave loading as those in rouge waves. Chen et al.[3] studied the scattering waves from focused wave and a surface piercing cylinder in computational fluid dynamics (CFD) method. They found the nonlinearity of scattering waves coincide with viscous around the cylinder. Ransley et al.[4] conducted a series of blind tests from fixed structure to floating body under focused waves, displayed the pros and cons of those various numerical methods in simulating focused wave-structure interactions.

Most studies rarely considered the effects of current in focused\freak waves interacted with cylinders. This might because generating waves over a current in a laboratory is a huge challenge[5-6], especially the focused wave. Feng et al.[7] applied a phase-manipulation method to do an experiment on focused wave-current interaction on a vertical cylinder. Yang et al.[8] applied smoothed particle method to simulate a breaking wave on the cylinder under a sheared current. Ghadirian et al.[9], Chen et al.[10] investigated a wave-current interaction and the inline force on a circular cylinder. Gong et al.[11] applied a hybrid method named qaleFOAM to simulate a

moving cylinder in focused waves. They made the cylinder moving with a speed instead of considering the current, thus ignored wave-current interaction. Agarwal et al.[12] collected and compared four numerical solvers on simulating the moving cylinder interacted with a focused wave.

In this paper, we apply an effective method to simulate a moving cylinder under a focused wave. The focused wave is generated using high-order spectral (HOS) method[13], and a CFD method with overset grid is coupled to extract the short-time focused wave information. The pressure and wave field around the moving cylinder is compared with experimental data to verify the coupled method, and the analysis of flow field is carried out.

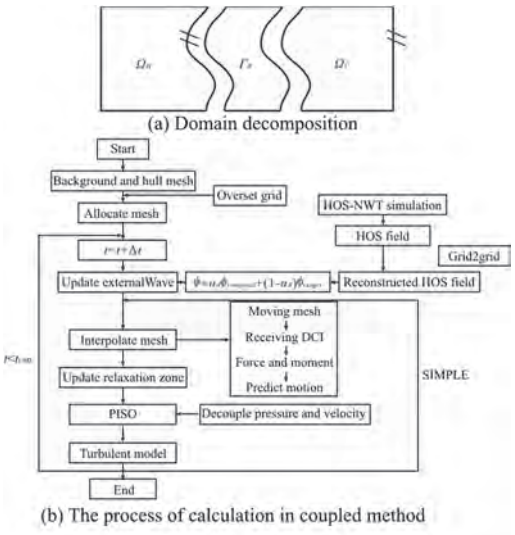

Fig. 1 The calculation process of the combined solver in naoe-FOAM-SJTU with overset grid

1. Numerical method

In this section, the numerical method adopted in this paper is introduced. We apply the coupled method of HOS, naoe-FOAM-SJTU with overset grid to achieve the simulation.

1.1 *Viscous solver*

Our in-house CFD solver naoe-FOAM-SJTU[14] is based on the open source software OpenFOAM with 6 DOF module, overset grids and turbulence models. The governing equations are:

$$\nabla \cdot \boldsymbol{U} = 0 \tag{1}$$

$$\frac{\partial \rho \boldsymbol{U}}{\partial t} + \nabla \cdot [\rho(\boldsymbol{U} - \boldsymbol{U}_g)\boldsymbol{U}] = -\nabla p_d - \boldsymbol{g} \cdot \boldsymbol{x} \nabla \rho \tag{2}$$

where $\boldsymbol{U}$ is velocity field, $\boldsymbol{U}_g$ is velocity of grid nodes, p_d is the dynamic pressure, $\boldsymbol{x}$ is the vector of the volumetric center position in one grid cell, $\boldsymbol{g}$ is the gravity and ρ is the density of the flow. The volume of fluid method with bounded techniques is applied.

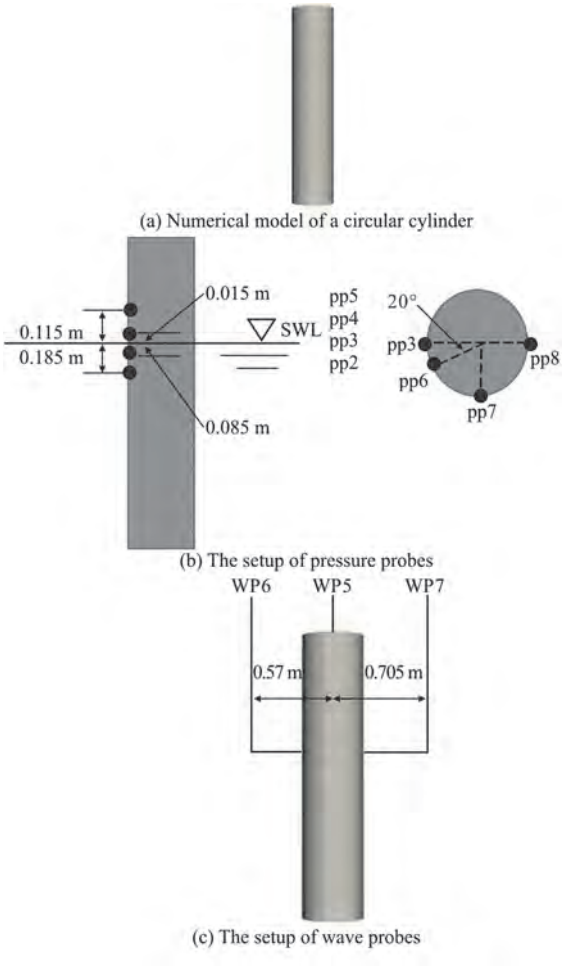

Fig. 2 The setup of numerical model and the pressure and wave probes

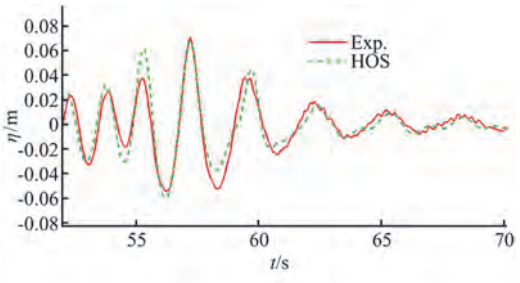

Fig. 3 (Color online) Comparison between HOS results and experimental results

In this paper, the turbulence model is chosen to be shear stress transfer (SST) k - ω [15]. The transform equations of turbulent kinetic energy and specific dissipation rate are:

$$\frac{\partial k}{\partial t}+\nabla\cdot(\boldsymbol{u}k)=\tilde{G}-\beta^{*}k\omega+\nabla\cdot[(\nu+\alpha_{k}\nu_{t})\nabla k] \tag{3}$$

$$\frac{\partial \omega}{\partial t}+\nabla\cdot(\boldsymbol{u}\omega)=\gamma S^{2}-\beta\omega^{2}+\nabla\cdot[(\nu+\alpha_{\omega}\nu_{t})\nabla\omega]+$$

$$(1-F_{1})CD_{k\omega} \tag{4}$$

where ν is the kinematic turbulent viscosity, ν_t is the turbulent eddy viscosity and F_1 is the function that combines k-ω model, standard k-ω model:

$$F_{1}=\tanh\left\{\min\left[\max\left(\frac{\sqrt{k}}{\beta^{*}\omega y},\frac{500\nu}{y^{2}\omega}\right),\frac{4\alpha_{\omega 2}k}{CD^{*}_{k\omega}y^{2}}\right]\right\}^{4} \tag{5}$$

$$CD^{*}_{k\omega}=\max\left(2\alpha_{\omega 2}\frac{1}{\omega}\nabla k\nabla\omega,10^{-10}\right) \tag{6}$$

where y is the wall distance.

In Eq. (3), $\tilde{G}$ can be described as

$$\tilde{G}=\min(G,c_{1}\beta^{*}k\omega),\quad G=\nu_{t}S^{2} \tag{7}$$

where S is the invariant measure of the strain rate.

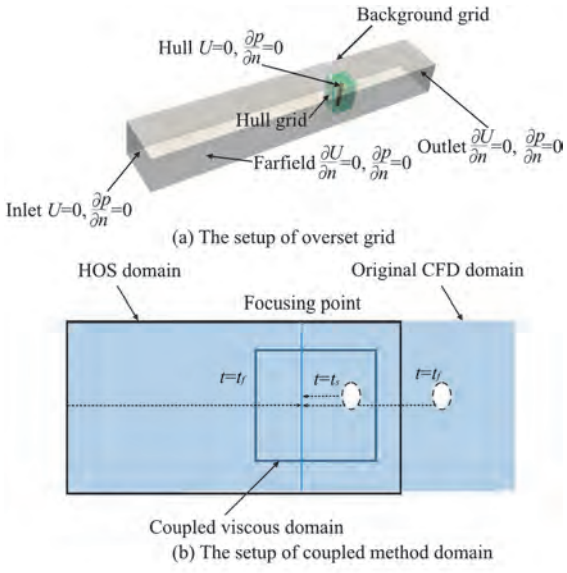

Fig. 4 (Color online) The setup of numerical simulation

Through the equation $\phi=F_1\phi_1+(1-F_1)\phi_2$ (ϕ stands for the parameter α_k, γ, β and α_ω in Eqs. (3), (4), ϕ_1 stands for the parameter α_{k1}, $\alpha_{\omega 1}$, β_1 and γ_1, ϕ_2 stands for the parameter α_{k2}, $\alpha_{\omega 2}$, β_2 and γ_2), all the parameters can be achieved. The values of all the parameters in above equations are $\alpha_{k1}=0.85034$, $\alpha_{k2}=1.0$, $\alpha_{\omega 1}=0.5$, $\alpha_{\omega 2}=0.85616$, $\beta_1=0.075$, $\beta_2=0.0828$, $\gamma_1=0.5532$, $\gamma_2=0.4403$, $\beta^{*}=0.09$ and $c_1=10$.

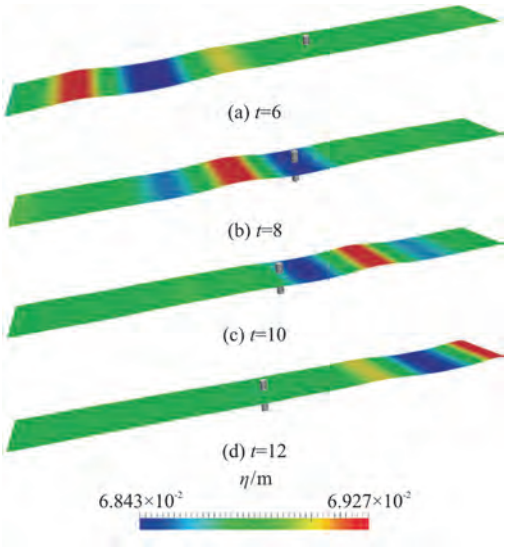

Fig. 5 (Color online) The wave field of moving cylinder in fixed computational domain

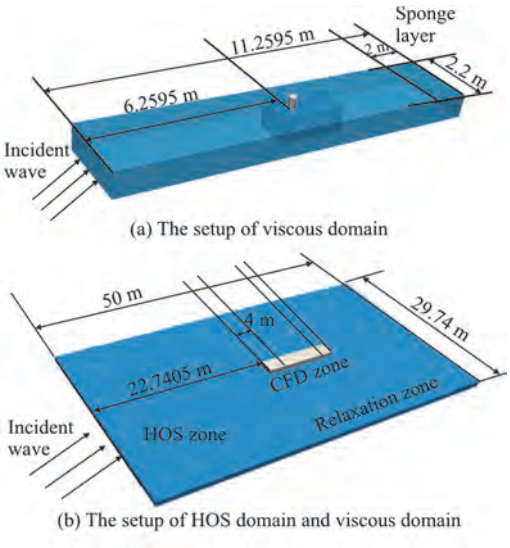

Fig. 6 (Color online) The setup of moving viscous domain and the whole computational domain

1.2 *HOS method*

The partial difference equation of HOS method scheme based on the dynamic and kinematic free surface boundary condition is[13]:

$$\eta_{t}+\nabla_{x}\phi^{s}\cdot\nabla_{x}\eta-(1+\nabla_{x}\eta\cdot\nabla_{x}\eta)\phi_{z}(\boldsymbol{x},\eta,t)=0 \tag{8}$$

$$\phi_t^s+\eta+\frac{1}{2}\nabla_x\phi^s\cdot\nabla_x\phi^s-\frac{1}{2}(1+\nabla_x\eta\cdot\nabla_x\eta)\phi_z^2(x,\eta,t)=-p_a \tag{9}$$

where ϕ^s is the surface potential function, p_a is the pressure, η is the wave elevation, t is the time, x and z stand for x and z direction.

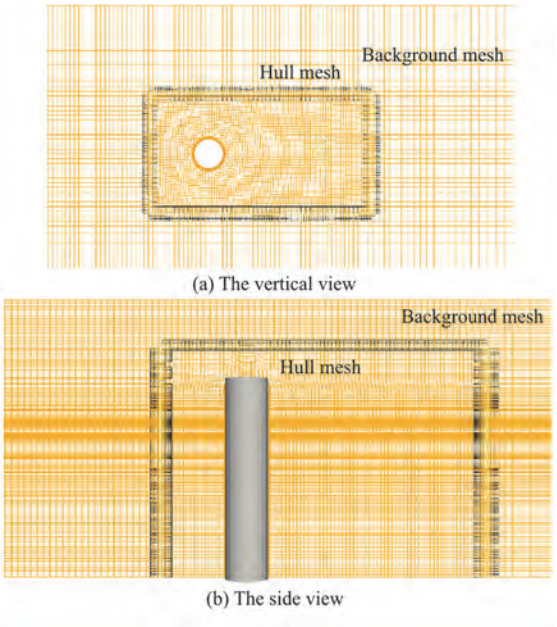

Fig. 7 (Color online) The overset mesh generation

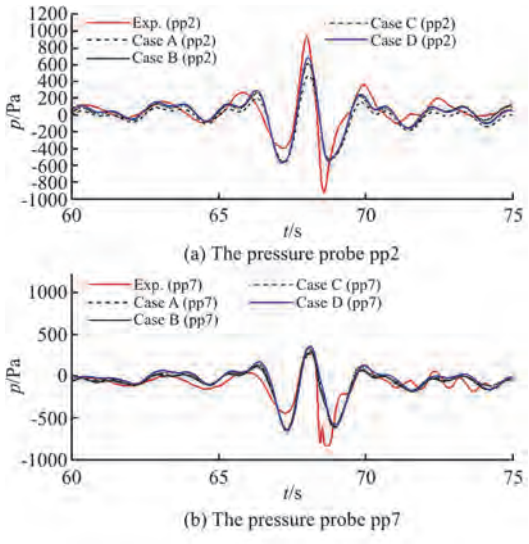

Fig. 8 (Color online) The mesh convergence study in different pressure probes

We utilized HOS-NWT[16] to generate focused wave in a method of flap wave maker. When we got the time history of wave elevation in wave tank, the Fourier transform gives complex number of wave elevation $\eta(f)$. With a delay of $e^{-k_i x_f}$ in phase, the wave can be regenerated where k_i is the wave number in each wave components, x_f is the focused position.

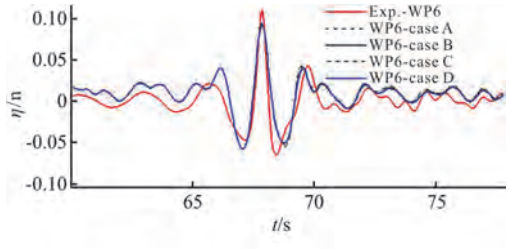

Fig. 9 (Color online) The mesh convergence study in wave probe wp6

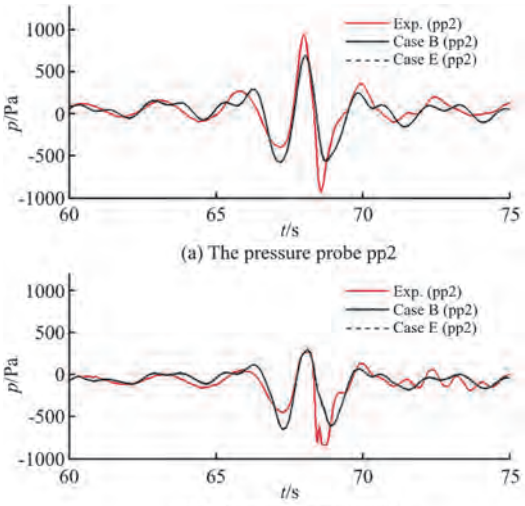

Fig. 10 (Color online) The time step convergence study in different pressure probes

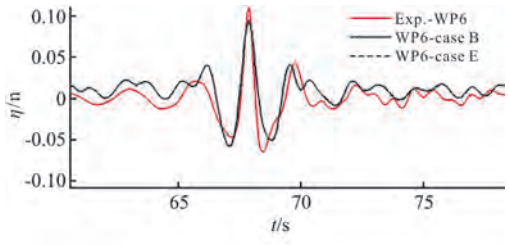

Fig. 11 (Color online) The time step convergence study in wave probe wp6

1.3 *Combined method*

We applied a computational decomposition method[17] to couple these two methods. To clearly illustrate the coupling method, Fig. 1(a) gives the way to deal with the interface of computational domains. Ω_H presents the reconstructed HOS field[18], Γ_R presents the interface, Ω_C is the CFD field. Therefore,

in the interface zone, there exists:

$$\boldsymbol{u}_R = \boldsymbol{u}_H, \quad x \in \Gamma_R \tag{10}$$

$$\eta_R = \eta_H, \quad x \in \Gamma_R \tag{11}$$

We applied relaxation scheme[19] in the interface, ϕ is the parameter of flow field

$$\phi = \alpha_R \phi_{\text{computed}} + (1-\alpha_R)\phi_{\text{target}} \tag{12}$$

The ϕ_{target} is from HOS field, ϕ_{computed} is computed from CFD zone. The relaxation weight α_R is exponential weight. The exponential weight has the following form[19]

$$\alpha_R = 1 - \frac{\exp \sigma^p - 1}{\exp 1 - 1} \tag{13}$$

The exponent p is set to 3.5 as default, σ is a local coordinate with relaxation zone.

Figure 1(b) shows the calculation process of the combined solver of naoe-FOAM-SJTU with overset grid. The detailed description of process can be found in previous work[20-21]. In this paper, we adopted frozen relaxation scheme to ensure the computational domain can move with the object.

2. Numerical simulation

In this numerical case, numerical model is chosen to be a circular cylinder. The wave condition is a unidirectional focused wave. The cylinder stands from a certain position and then starts moving towards the peak of the focused wave at a speed of 0.25 m/s.

2.1 *Numerical setup*

The diameter of the circular cylinder is 0.22 m, the height is 1.055 m, as shown in Fig. 2(a).

The focused wave model is a unidirectional focused wave composed of 32 wave components, with a wave frequency range from $f_1 = 0.34$ Hz to $f_{\max} = 1.02$ Hz. The focused time is 38s, and the

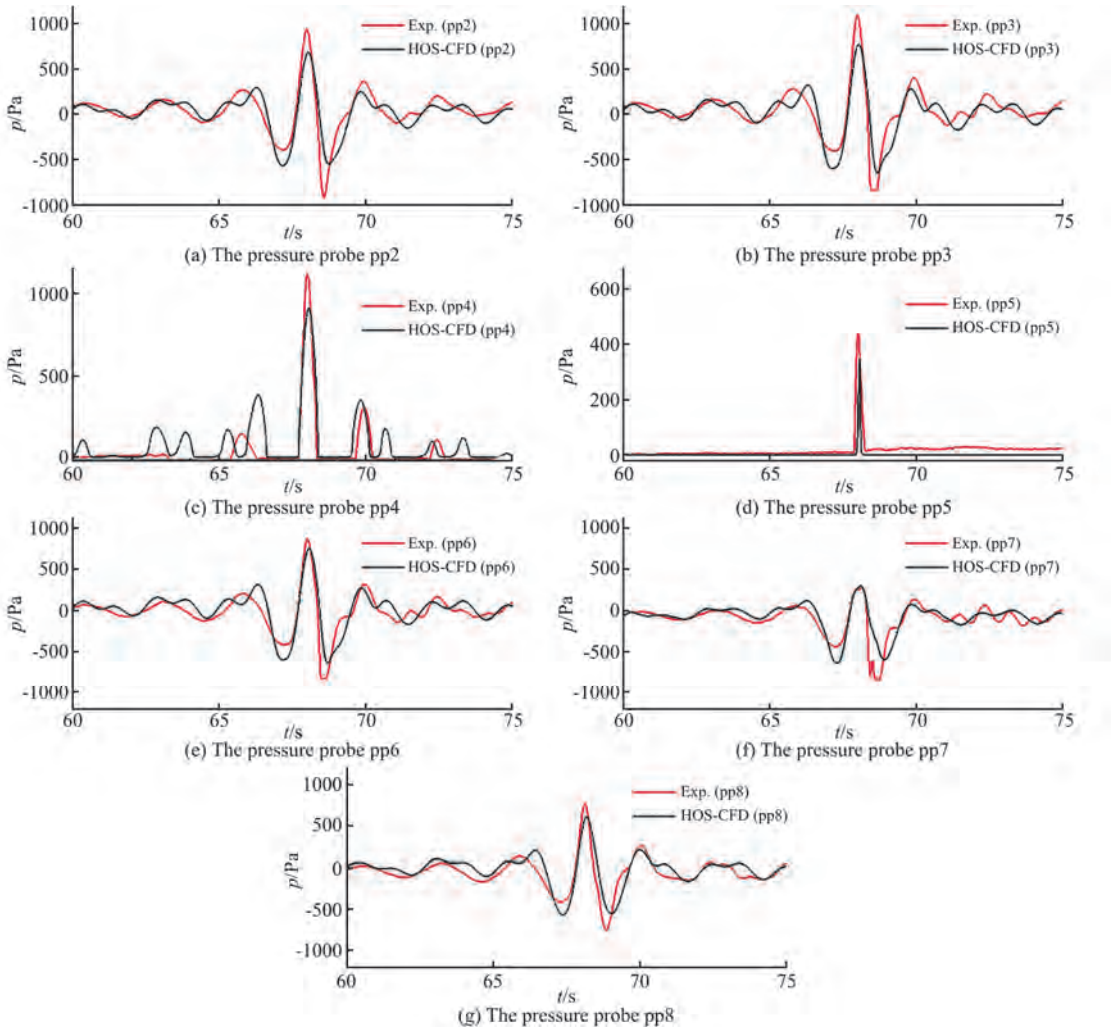

Fig. 12 (Color online) The comparison between numerical results and experimental data

focused point is 23 m away from the wave making position. The experiment applies the piston wave making method for wave generation, and the depth of the water tank is 0.7 m[22].

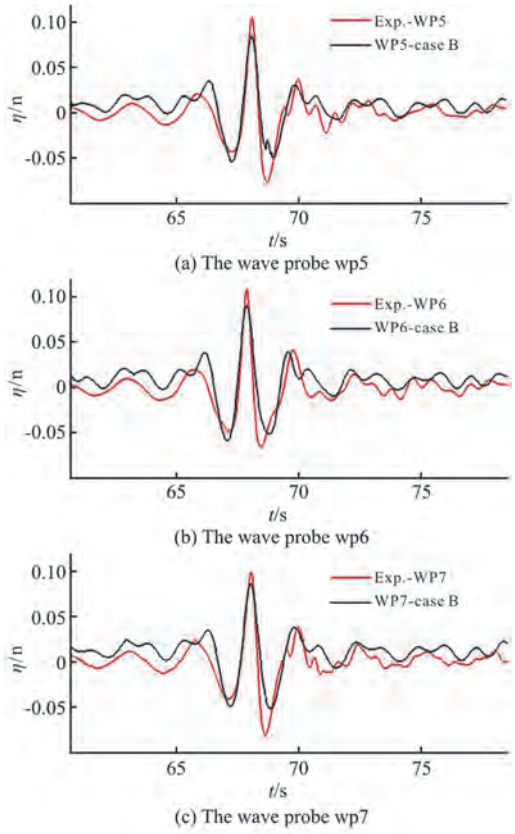

Fig. 13 (Color online) The comparison of wave probes between numerical results and experimental data

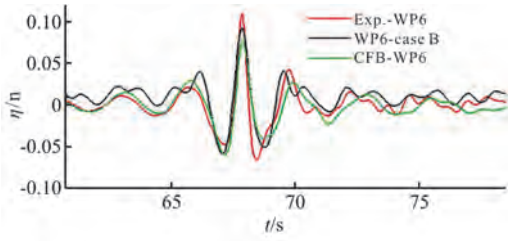

Fig. 14 (Color online) Comparison of coupled method with original CFD method

In order to compare with the experimental results, seven pressure probes are set on the circular cylinder, with four probes located at an angle of 0° from the incident wave. The distance between the probes and the bottom of the water tank is 0.515 m, 0.615 m, 0.715 m and 0.815 m. The other three are at angles of 20°, 90° and 180° from the incident wave, and at a distance of 0.615 m from the bottom of the wave tank, as shown in Fig. 2(b). Meanwhile, Fig. 2(c) illustrates three wave probes moving with the cylinder, they are at the distance of 0.57 m in the front of the cylinder center, on the cylinder center and behind the cylinder center.

Considering the complex flow field around the cylinder, the turbulence model is chosen to be the Reynolds averaged Navier-Stokes SST k-ω model. The time integration scheme adopts the second order Crank-Nicholson scheme, the convective term in the momentum equation adopts the mixed linear upwind stabilized for transport (LUST) scheme, and the convective term in the turbulent transport equation adopts the total variation diminshing scheme. The viscous term adopts the central differencing scheme.

2.2 *Validation*

Firstly, we generate the wave field based on HOS-NWT. The experiment results didn't include the wave elevation in empty wave tank, we adopt the wave probe at $x = 4.975$ m as initial wave elevation, where the wave is not influenced by the scattering wave from cylinder.

The computational domain in HOS method is set as: $L_x = 50$ m , $L_y = 29.74$ m , The water depth $h = 0.7$ m , the HOS order $M = 5$, the discrete point $N_x = 512$, $N_z = 33$. The CPU time is 75 s with one core. Figure 3 illustrates the comparison of wave elevation between experimental results and HOS results. The wave crest and through agrees well with that in experimental data.

Figure 4 displays the numerical setup of the moving cylinder. In this case, the cylinder moves forward with a certain speed, thus overset grid is adopted. Figure 4(a) shows the layout of boundary conditions with overset grid method. Figure 4(b) shows the layout comparison between present method and original CFD method. If we adopted traditional CFD methods or other global solving methods, the calculation domain represented by light blue blocks in the figure is required, which includes the distance of the focused wave propagation and the long-time cylinder walking. This will require a large computational domain and huge computing resources. In this paper, the HOS region considers the focused distance of the focused wave, while the CFD region considers the cylinder motion distance. By selecting the coupling region near the formation of the focused wave, the cylindrical motion time can be greatly reduced, thus the computational domain size and time in the CFD region is reduced.

For the object with the forward speed, there are two ways to calculate using the overset grid method. One is to fix the computational domain and move the object forward, as shown in Fig. 5. It can be seen that with the speed of 0.25 m/s, even if the simulation is only conducted near the focused position, it is still

Table 1 Main parameters of test cases

Name	Number of background grid number×10^6	Number of hull grid number×10^6	Number of total grid number×10^6	Time step/s
Case A	49	25	74.8	0.002
Case B	161	72	232	0.002
Case C	529	197	726	0.001
Case D	49	72	121	0.002
Case E	161	72	232	0.001

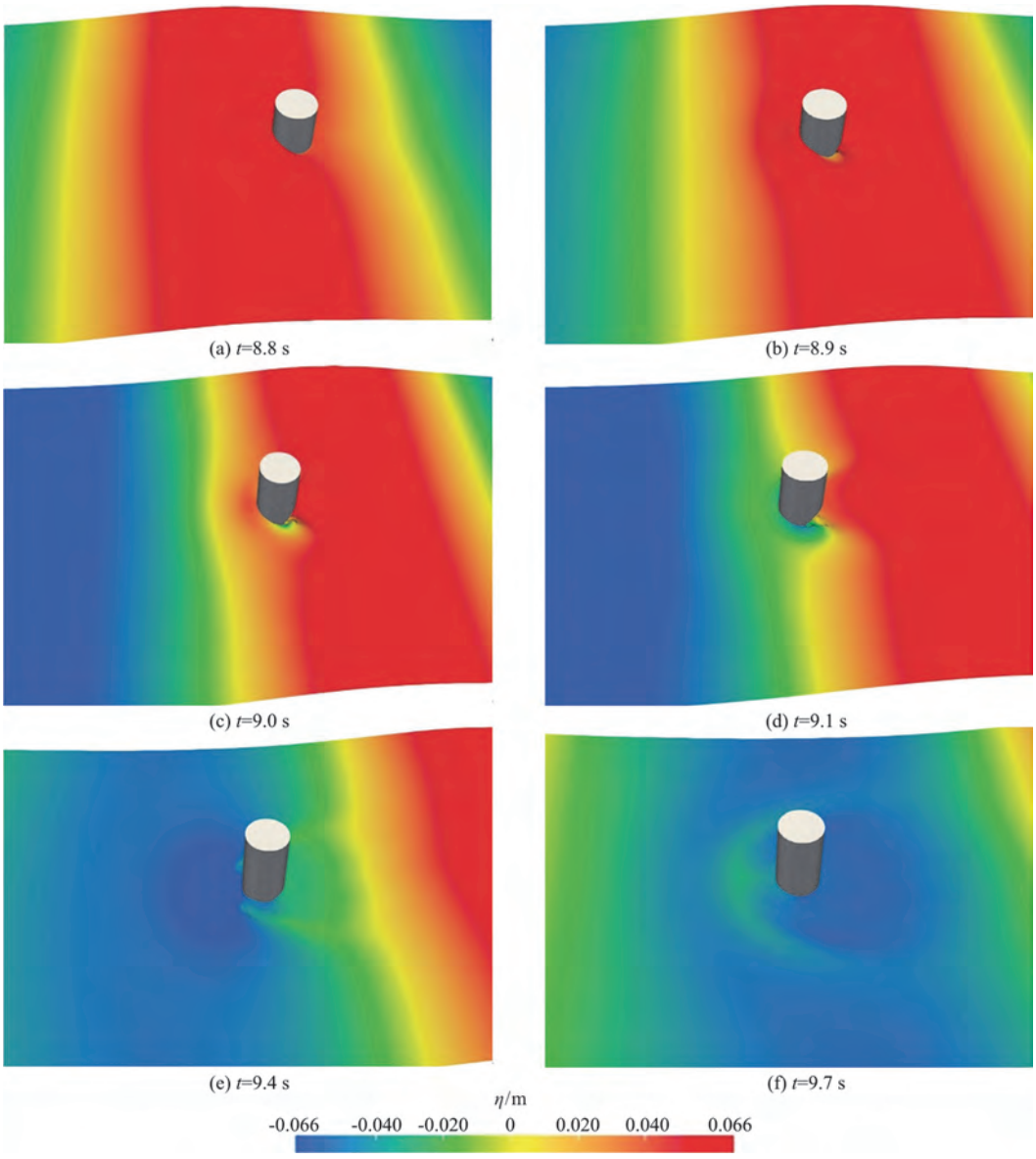

Fig. 15 (Color online) The wave fields around cylinder

need to add at least 5 m length to the calculation domain. Therefore, in order to save resources to a greater extent, we applied the way that viscous computational domain moves with the object.

The viscous CFD computational domain moves in the HOS wave field at the same speed of cylinder, while the relative position of the cylinder and the computational domain remains unchanged. Figure 6 shows the size of the computational domain and its layout in the HOS domain. The computational domain size is $-6.2595\ \text{m} < x < 5\ \text{m}$, $-1.1\ \text{m} < y < 1.1\ \text{m}$ and $-0.7\ \text{m} < z < 0.7\ \text{m}$. The length of relaxation zone is $-6.2595\ \text{m} < x_i < -2.2595\ \text{m}$, $3\ \text{m} < x_o < 5\ \text{m}$ (x_i

and x_o represent the inlet and outlet relaxation zones respectively). The distance from the viscous domain to the HOS domain is $x = 29$ m, $y = 15$ m. The simulation time is 20 s.

The mesh generation tools BlockMesh and snappyHexMesh in OpenFOAM are adopted for background and cylinder mesh generation. The mesh is refined on the free surface and around the cylinder. In order to ensure complete vortex shedding during the movement of the cylinder, the mesh is refined in the length of four times of cylinder diameters behind the cylinder in the object grid as shown in Fig. 7.

Five different cases with different grid number and time steps are carried out for convergence simulation. The parameters of background grid, hull grid, and total grid quantity for each case are shown in Table 1. Case A has 70 grid number per wavelength and 22 grid number per wave height, case B has 100 grid number per wavelength and 32 grid number per wave height, case C has 141 grid number per wavelength and 45 grid number per wave height.

The comparison among the time history of the two pressure probes under the four cases A, B, C and D with the experimental results are shown in Fig. 8. It can be seen that among the two pressure probes, the results of case A has the largest discrepancy from the experimental results. The results of cases B, C are very similar. The results of case D are consistent with those of case B at pressure probe pp2, while the results of Case B are closer to the experimental results at pp7. cases B, D have the same grid number around the object. It can be seen that since the background grid number in case D is selected, the wave converges and there is no numerical dissipation due to the wave propagation. The finer background grid number in case C doesn't bring the values of the pressure probes closer to the experimental values. This may be due to the fact that the grid already satisfies wave propagation in case B, and on the other hand, it may require a smaller time step to obtain more accurate results.

The comparison of wave elevation between the wave probe wp6 around the cylinder and the experimental data under four cases is displayed in Fig. 9. Similar to that in pressure probes, the background grid number in cases A, D already meets the needs of wave propagation. Therefore, the results of the time history of wave elevation obtained from these four cases are very close.

Figures 10, 11 show the comparison of pressure probes and wave probes between cases B, E with the

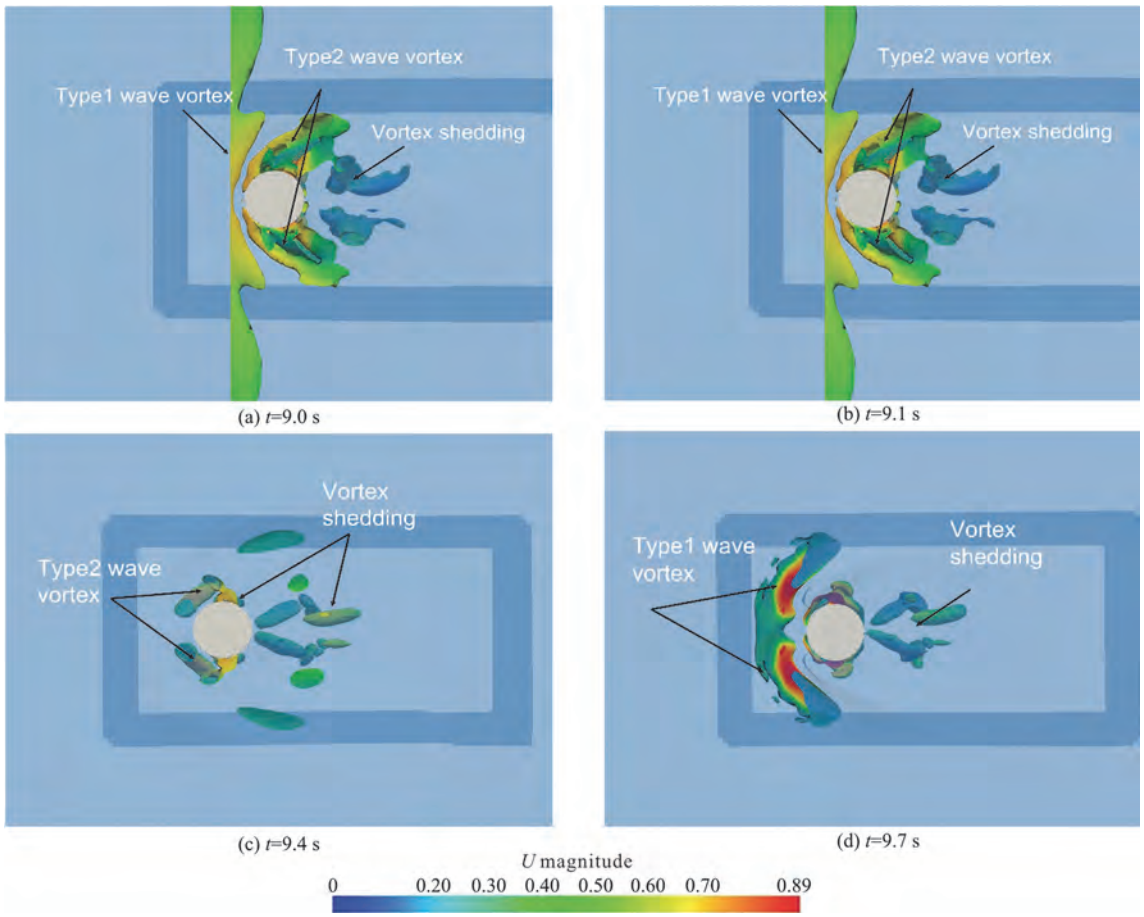

Fig. 16 (Color online) The vortex in wave field

same grid setting in different time steps. The results of both pressure and wave elevation are basically the same, indicating that the time step of 0.002 s already conforms to the current simulation. Therefore, case B is used for the subsequent simulation and analysis.

The comparison between the numerical results and the experimental data with 7 pressure probes is shown in Fig. 12. It can be seen that the numerical results and experimental results are in good agreement at pressure probes pp6, pp7 and pp8. The numerical error at pp7 is about 3%, while the numerical errors of the other two probes are all within 25%. The numerical results of the four pressure probes at the head wave side are smaller than that in experimental values. The discrepancy may come from the way that pressure captured. The pressure results all come from a certain point on the cylinder surface, which is the grid node. Therefore, errors may occur due to moving of grid nodes during simulation. In the pressure probes at angles from head wave side, the numerical results are

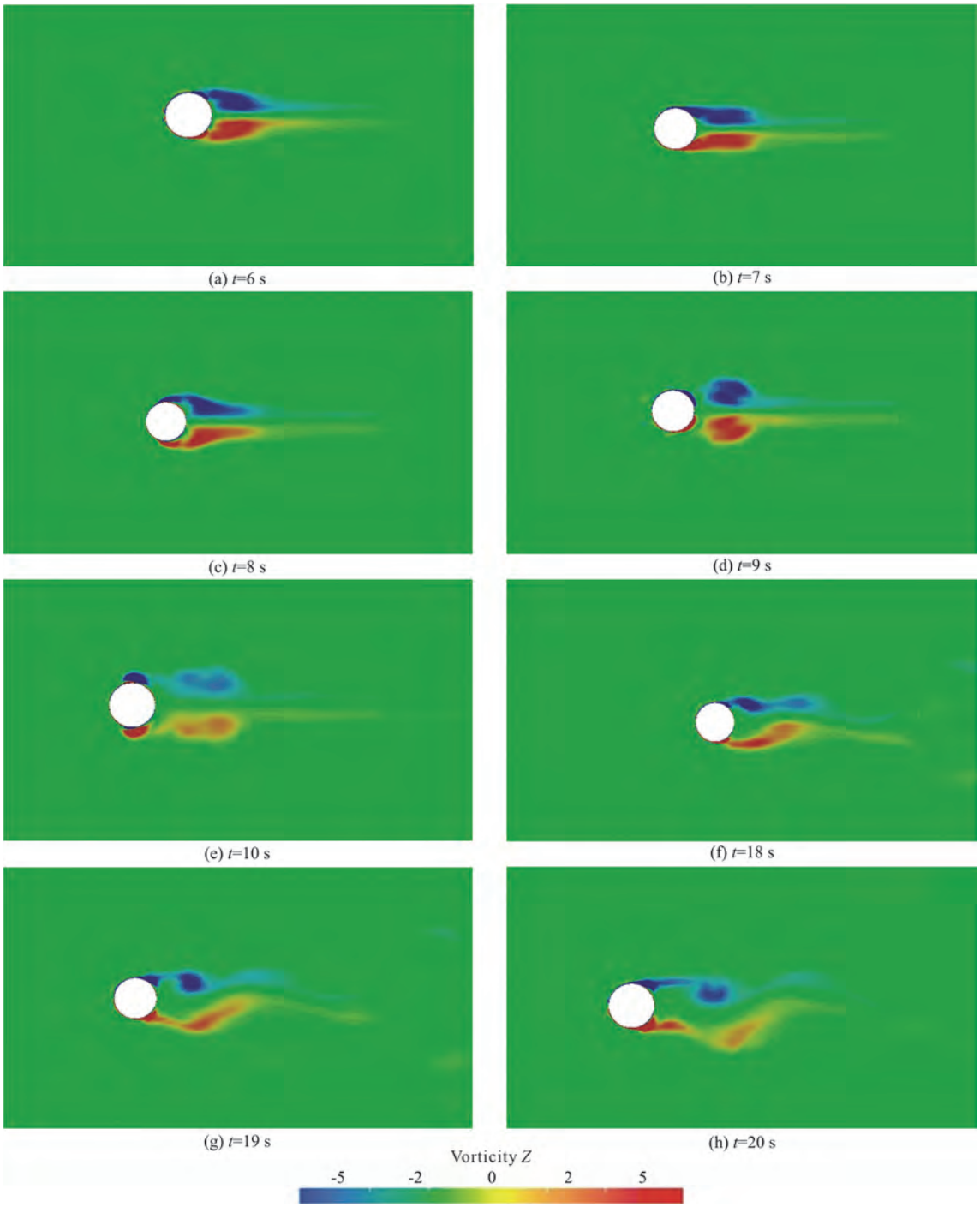

Fig. 17 (Color online) The vortex around cylinder at $z = -0.6$ m

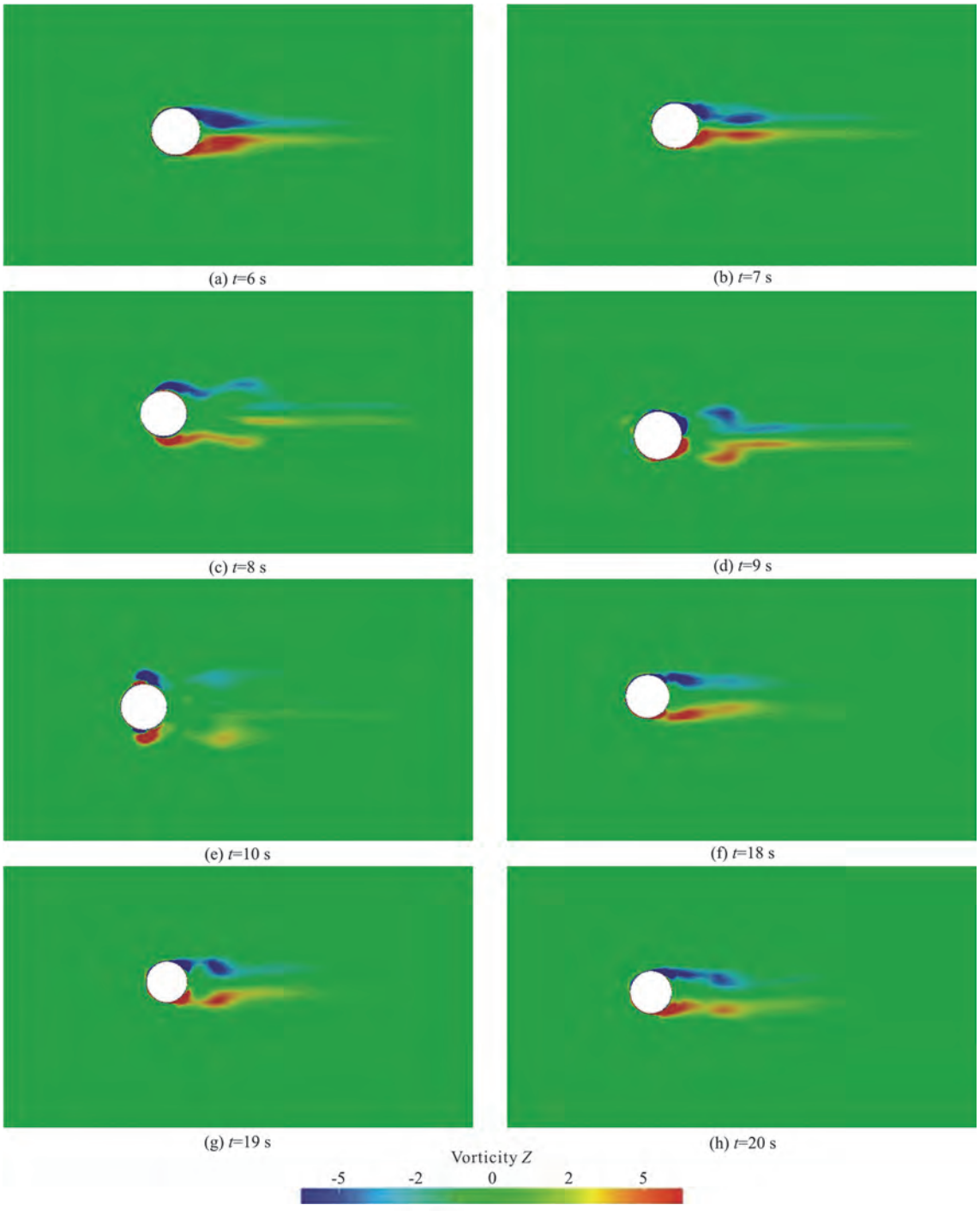

Fig. 18 (Color online) The vortex around cylinder at $z = -0.1$ m

in good agreement with the experimental values, indicating that the flow field around the cylinder can be well simulated and captured.

Figure 13 shows the comparison between numerical results and the experimental data with wave elevation at the front, back, and center of the cylinder. The numerical results of wave climb in front of and at the center of the cylinder are slightly smaller than the experimental values, and the numerical results of wave climb behind the cylinder are closer to the experimental values.

The original CFD method needs large computational domain and resources as we mentioned before. We compared our coupled method with that in original CFD method[16], as shown in Fig. 14. Through reducing computational domain and simulation time, the accuracy of the numerical results increases and CPU time reduces 65%.

3. Flow field analysis

3.1 *scattering wave*

Figure 15 shows the flow field around the cylinder when it passes through the focused wave. When $t = 8.8$ s, the cylinder encounters with the crest of the focused wave. When $t = 8.9$ s, a roll-up of free surface is captured on the backside of the cylinder. At the time of $t = 9$ s, a type 1 concentric circular scattering wave surface appeared at the head of the cylinder, and a type 2 scattering wave surface appeared on both sides of the cylinder. At the same time, the roll-up behind the cylinder is more obvious, and a breaking phenomenon is captured. At the moment of $t = 9.1$ s, the moving cylinder leaves the wave crest, while the wave climb on the back cylinder continues, and there still exists waves breaking and rolling on both sides of the cylinder. At $t = 9.4$ s, the cylinder encounters with the trough of focused wave, and an obvious Coanda effect appears on the side of the cylinder with rise of free surface. This wave surface promotion gradually eliminates until $t = 9.7$ s, and the wave surface promotions on both sides of the cylinder converge at the front of the cylinder, forming a type 1 scattering wave surface again.

Figure 16 illustrates the vortex around the cylinder. It can be seen that with the existence of scattering wave, the vortex around the cylinder shows corresponding type with the scattering waves. Meanwhile, due to the uniform speed of the cylinder, the vortex begins to detach at $t = 9.0$ s, stretch at $t = 9.4$ s.

3.2 *Vortex shedding*

Figure 17 illustrates vortex shedding at $z = -0.6$ m. At this space, the free surface and waves have no effect on the vortex, thus the overall vortex shedding is roughly the same as that in uniform flow passes through cylinder. At $t = 6$ s, two vortices form behind the cylinder. As the cylinder moves forward, the vortex shedding begins to appear at $t = 8$ s and exhibit a completely detached form at $t = 9$ s. After the cylinder continues to move forward for 9 s, that is, at $t = 18$ s, the alternative vortex shedding behind the cylinder is observed.

Figure 18 illustrates vortex shedding at $z = -0.1$ m. At this cross-section, it is very close to the free surface, and the vortex shedding of the cylinder is not only affected by the free surface, but also by the wave velocity. It can be seen that at $t = 6$ s, two vortices are also formed behind the cylinder, and at this time, the two vortices extend along the wave propagation direction under the influence of wave velocity. The vortex exhibits a completely different shape from the vortex at $z = -0.6$ m starting from $t = 7$ s. The vortex at the free surface becomes slender under the action of wave velocity, and the vortex that just falls off is immediately stretched or even wiped out. Therefore, at $t = 18$ s, there is still no alternative vortex shedding observed.

4. Conclusions

This paper applies an effective method coupled HOS and CFD method with overset grid to solve the hydrodynamic problem of a moving cylinder in a unidirectional focused wave. By applying overset grid technology, the viscous computational domain and the cylinder move forward simultaneously in the HOS wave field. The accuracy of the calculation results is verified by comparing the time history of the pressure probes and wave probes on the cylindrical surface with the experimental results. We analyze the scattering wave field around the cylinder, and two classical scattering wave types are found when the cylinder passing through the focused wave. The moving cylinder doe not change the scattering wave type, but strength it. The type-2 scattering wave breaks at the backside of the cylinder due to the object's uniform speed.

The vortex shedding at the bottom and near free surface of a cylinder is discussed. Due to the presence of waves at the free surface, the detached vortices cannot form alternative vortex shedding. At the bottom, as it is not disturbed by the free surface, a clear phenomenon of alternative vortex shedding can be observed.

Acknowledgement

(This research received other funding agency in the public, commercial, or not-for-profit sectors.)

Compliance with ethical standards

Conflict of interest: The authors declare that they have no conflict of interest. De-cheng Wan is an editorial board member for the Journal of Hydrodynamics and was not involved in the editorial review, or the decision to publish this article. All authors declare that there are no other competing interests.

Ethical approval: This article does not contain any studies with human participants or animals performed by any of the authors.

Informed consent: Informed consent was obtained from all individual participants included in the study.

References

[1] Sriram V., Agarwal S., Schlurmann T. Laboratory study on steep wave interactions with fixed and moving cylinder [J]. *International Journal of Offshore and Polar Engineering*, 2021, 31(1): 19-26.

[2] Mohseni M., Esperanca P. T., Sphaier S. H. Numerical study of wave run-up on a fixed and vertical surface-piercing cylinder subjected to regular, non-breaking waves using OpenFOAM [J]. *Applied Ocean Research*, 2018, 79: 228-252.

[3] Chen S., Zhao W., Wan D. On the scattering of focused wave by a finite surface-piercing circular cylinder: A numerical investigation [J]. *Physics of Fluids*, 2022, 34(3): 035132.

[4] Ransley E., Yan S., Brown S. et al. A blind comparative study of focused wave interactions with floating structures (CCP-WSI Blind Test Series 3) [J]. *International Journal of Offshore and Polar Engineering*, 2020, 30(1): 1-10.

[5] Saincher S., Sriram V., Agarwal S. et al. Experimental investigation of hydrodynamic loading induced by regular, steep non-breaking and breaking focused waves on a fixed and moving cylinder [J]. *European Journal of Mechanics-B/Fluids*, 2022, 93: 42-64.

[6] Vested M. H., Carstensen S., Christensen E. D. Experimental study of wave kinematics and wave load distribution on a vertical circular cylinder [J]. *Coastal Engineering*, 2020, 157: 103660.

[7] Feng X., Taylor P. H., Dai S. et al. Experimental investigation of higher harmonic wave loads and moments on a vertical cylinder by a phase-manipulation method [J]. *Coastal Engineering*, 2020, 160: 103747.

[8] Yang Y., Stansby P. K., Rogers B. D. et al. The loading on a vertical cylinder in steep and breaking waves on sheared currents using smoothed particle hydrodynamics [J]. *Physics of Fluids*, 2023, 35(8): 087132 .

[9] Ghadirian A., Vested M. H., Carstensen S. et al. Wave-current interaction effects on waves and their loads on a vertical cylinder [J]. *Coastal Engineering*, 2021, 165: 103832.

[10] Chen L. F., Stagonas D., Santo H. et al. Numerical modelling of interactions of waves and sheared currents with a surface piercing vertical cylinder [J]. *Coastal Engineering*, 2019, 145: 65-83.

[11] Gong J., Yan S., Ma Q. et al. Numerical simulation of fixed and moving cylinders in focusing wave by a hybrid method [J]. *International Journal of Offshore and Polar Engineering*, 2021, 31(1): 102-111.

[12] Agarwal S., Saincher S., Sriram V. et al. A comparative study on the nonlinear interaction between a focusing wave and cylinder using state-of-the-art solvers: Part B [J]. *International Journal of Offshore and Polar Engineering*, 2021, 31(1): 11-18.

[13] Dommermuth D. G., Yue D. K. P. A high-order spectral method for the study of nonlinear gravity waves [J]. *Journal of Fluid Mechanics*, 1987, 184: 267-288.

[14] Wang J. H., Wan D. C. CFD investigations of ship maneuvering in waves using naoe-FOAM-SJTU solver [J]. *Journal of Marine Science and Application*, 2018, 17(3): 443-458.

[15] Menter F. R. Two-equation eddy-viscosity turbulence models for engineering applications [J]. *AIAA Journal*, 1994, 32(8): 1598-1605.

[16] Ducrozet G., Bonnefoy F., Touz´e D. L. et al. A modified high-order spectral method for wavemaker modeling in a numerical wave tank [J]. *European Journal of Mechanics-B/Fluids*, 2012, 34: 19-34.

[17] Zhong W. J., Wang W. T., Wan D. C. Coupling potential and viscous flow models with domain decomposition for wave propagations [J]. *Journal of Hydrodynamics*, 2022, 34(5): 826-848.

[18] Li Z., Deng G., Queutey P. et al. Comparison of wave modeling methods in CFD solvers for ocean engineering applications [J]. *Ocean Engineering*, 2019, 188: 106237.

[19] Jacobsen N. G., Fuhrman D. R., Fredsøe J. A wave generation toolbox for the open-source CFD library: OpenFoam® [J]. *International Journal for Numerical Methods in Fluids*, 2012, 70(9): 1073-1088.

[20] Zhuang Y., Wan D. C. Parametric study of a new HOS-CFD coupling method [J]. *Journal of Hydrodynamics*, 2021, 33(1): 43-54.

[21] Zhuang Y., Wang G., Wan D. C. et al. Numerical simulations of FPSO with sloshing tanks in a random freak waves [J]. *Journal of Hydrodynamics*, 2022, 34(3): 491-498.

[22] Yan S., Ma Q. W., Sriram V. et al. Numerical and experimental studies of moving cylinder in uni-directional focusing waves [C]. *ISOPE International Ocean and Polar Engineering Conference*, Big Island, Hawaii, USA, 2015.